Ab-initio and crystal field studies of the Mn< sup> 4+</sup>-doped Ba< sub> 2</sub> LaNbO< sub> 6</sub> double-perovskite

ARTICLE · JANUARY 2012

READS
45

2 AUTHORS:

Alok M Srivastava
General Electric
195 PUBLICATIONS **1,880** CITATIONS
SEE PROFILE

Mikhail G Brik
University of Tartu
397 PUBLICATIONS **2,387** CITATIONS
SEE PROFILE

Journal of Luminescence 132 (2012) 579–584

Contents lists available at SciVerse ScienceDirect

Journal of Luminescence

journal homepage: www.elsevier.com/locate/jlumin

Ab initio and crystal field studies of the Mn^{4+}-doped Ba_2LaNbO_6 double-perovskite

A.M. Srivastava [a,*], M.G. Brik [b]

[a] GE Global Research, K1-4A22, GE Global Research, One Research Circle, Niskayuna, NY 12309, USA
[b] Institute of Physics, University of Tartu, Riia 142, Tartu 51014, Estonia

ARTICLE INFO

Article history:
Received 15 April 2011
Received in revised form
7 September 2011
Accepted 12 September 2011
Available online 29 September 2011

Keywords:
Perovskite
Ba_2LaNbO_6
Mn^{4+}
Ab initio DFT based calculations
Energy level scheme

ABSTRACT

A detailed study using the ab initio DFT-based calculations of the electronic and optical properties of pure and Mn^{4+} doped Ba_2LaNbO_6 is presented in this paper. Comparison of the calculated electronic bands structure, density of states diagrams, and dielectric functions for the pure and doped crystal reveals the changes induced by the Mn^{4+} impurity ions. In addition, the energy levels of the Mn^{4+} ion in the ordered perovskite Ba_2LaNbO_6 are calculated by the exchange charge model (ECM) of crystal field theory and compared with the experimental data that has been presented in the literature. The calculated Mn^{4+} energy levels are in good agreement with the experimental spectra. Additionally, the excitation band shapes of the $^4A_{2g}(^4F)$–$^4T_{2g}(^4F)$ and $^4A_{2g}(^4F)$–$^4T_{1g}(^4F)$ transitions are modeled to estimate the zero-phonon lines (ZPL) positions and the effective number of phonons, which are involved in the corresponding excitation transition. The results of our calculations yield the crystal field parameter of $Dq=1780\ cm^{-1}$ and Racah parameters $B=670$ and $C=3290\ cm^{-1}$, with $C/B=4.9$ for the Mn^{4+} ion in the double-perovskite Ba_2LaNbO_6.

1. Introduction

The spectroscopy of Mn^{4+}-doped crystalline host materials is of continuing interest for applications in the fields of lighting, holographic recording, optical data storage, and dosimetry. The deep red luminescence of the Mn^{4+} ($3d^3$) ion finds commercial use in lighting industry. The classic phosphor, Mg-germanate:Mn^{4+} has been widely applied as a color correcting phosphor in High Pressure Mercury Vapor Lamps (HPMVL) and in fluorescent lamps for providing light for plant growth [1–3]. More recently, the Mn^{4+} luminescence in fluoride host lattices has been patented for use in white light generating phosphor blends in LED devices [4]. Perovskites such as $YAlO_3$ and activated with Mn^{4+} have been evaluated as potential materials for holographic recording and optical data storage [5,6], for laser application [7], and as materials for thermoluminescence dosimetry [8].

Tanner and Pan [9] have recently reported on the optical properties of the $[MnO_6]^{8-}$ cluster in the double-perovskite, Ba_2LaNbO_6. The goal of the present paper is to provide a consistent crystal field analysis of the energy levels of the Mn^{4+} ion in the double-perovskite, Ba_2LaNbO_6:Mn^{4+}. We have used the ab initio DFT-based calculations for elucidating the structural, electronic, and optical properties of both pure and Mn^{4+}-doped Ba_2LaNbO_6. The energy levels of the Mn^{4+} ion have been calculated and the results compared with the experimental spectroscopic data, which has been presented in Ref. [9]. Additionally, the excitation band shapes were modeled with an aim of evaluating the main parameters of the electron–vibrational interaction (EVI) between the electronic states of the Mn^{4+} ions and vibrations of the host's crystal lattice.

2. Crystal structure and first-principles computational details

The crystal structure of the host lattice Ba_2LaNbO_6 is that of a tetragonally distorted perovskite. This double perovskite crystallizes in the space group I2/m [10] with lattice constants a, b, c (all in Å) of 6.14448, 6.09131, 8.60400, $\beta=90.348^\circ$ and with two formula units in a unit cell [11]. The crystal structure of Ba_2LaNbO_6 crystal is shown in Fig. 1. The structure can be described as a chain of the oxygen octahedra (with Nb ions at the center), slightly tilted with respect to the z axis; the La ions are in the same planes as the Nb ions (parallel to the a and b axes), the Ba ions also form parallel layers in the space between the (La, Nb) planes.

The DFT-based calculations were performed using the CASTEP module [12] of Materials Studio 4.0. To identify and highlight the changes in the electronic and structural properties produced by impurity, the calculations were first performed on the

* Corresponding author. Tel.: +1 518 387 7535; fax: +1 518 387 4820.
E-mail addresses: srivastava@crd.ge.com (A.M. Srivastava), brik@fi.tartu.ee (M.G. Brik).

0022-2313/$ - see front matter © 2011 Published by Elsevier B.V.
doi:10.1016/j.jlumin.2011.09.017

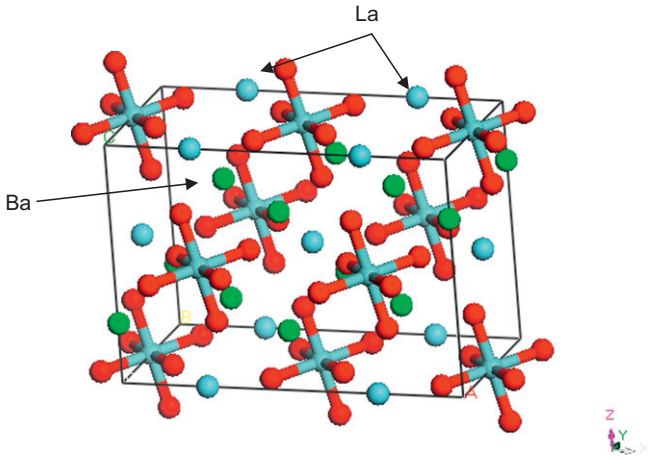

Fig. 1. The crystal structure of Ba_2LaNbO_6. Chemical bonds between the Nb and O ions are shown; the La ions are on the edges of supercell ($2\times1-1$); the Ba ions are inside the supercell.

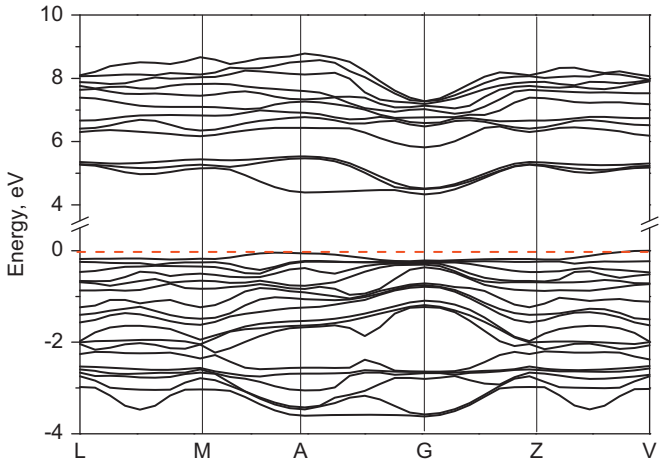

Fig. 2. Calculated band structure of pure Ba_2LaNbO_6.

unactivated (ideal) crystal. The total plane-wave pseudopotential method forms a basis of the CASTEP calculations. The exchange–correlation effects were treated within the generalized gradient approximation (GGA) with the Perdew–Burke–Ernzerhof functional [13]. The Monkhorst–Pack scheme k-points grid sampling was set at $5\times5\times4$ for the Brillouin zone for pure Ba_2LaNbO_6 and $2\times4\times3$ for Mn^{4+}-doped host with $2\times1\times1$ supercell. The plane-wave basis set energy cutoff was set at 340 eV for both cases. The convergence parameters were as follows: total energy tolerance—1×10^{-5} eV/atom, maximum force tolerance 0.03 eV/Å, and maximum stress component 0.05 GPa. The electronic valence configurations for each atomic species were: Ba: $5s^25p^66s^2$; La: $5s^25p^65d^16s^2$; Nb: $4s^24p^64d^45s^1$; O: $2s^22p^4$; Mn: $3d^54s^2$.

The optimized lattice constants for the pure host were obtained as follows (in Å): $a=6.208393$; $b=6.16256$; $c=8.70924$, $\beta=90.775^\circ$, with the largest deviation between the experimental and calculated lattice constant of 1.2% only.

The optimized crystal lattice constants for the Mn^{4+}-doped crystal were (in Å): $a=6.18977$; $b=6.112402$; $c=8.666489$, $\beta=90.866^\circ$. We note here that the lattice constants of the Mn^{4+}-doped crystal are slightly decreased in comparison with the pure host, which can be explained by a smaller ionic radius of Mn^{4+} ion in comparison with that one of Nb^{5+} (0.78 and 0.68 Å, respectively [14]). The ionic radii of the six-fold coordinated sites, Nb^{5+} and La^{3+} are 0.78 and 1.185 Å, respectively. Note that charge compensation is required for the substitution of Mn^{4+} on the Nb^{5+} site. It may be argued that the Mn^{4+} distributes itself equally between the La^{3+} and Nb^{5+} sites (despite the considerable ionic radii differences between La^{3+} and Mn^{4+}) to provide for the necessary charge compensation. In our calculations and discussions it is assumed that the Mn^{4+} occupies the Nb^{5+} site in the Ba_2LaNbO_6 lattice.

After geometry optimization, the calculations pertaining to the band structure, full and partial density of states (DOS), optical properties and Mulliken charges were performed for both unactivated and Mn^{4+} activated crystals.

3. Electronic and optical properties of pure Ba_2LaNbO_6

The calculated electronic band structure of Ba_2LaNbO_6 is shown in Fig. 2. The band gap appears to be of an indirect character. Its calculated value was about 3.13 eV, which was corrected by the scissor operator [15] of 1.2 eV to adjust it to the experimental estimation of 4.3 eV, which corresponds to the absorption edge of the isostructural double perovskite, Ba_2GdNbO_6 [16].

It can be immediately noticed from Fig. 2 that all electronic states in the conduction band exhibit well-pronounced dispersion in all directions. The valence band states at its top are very flat (which would show a very high effective mass of the holes in the valence band). However, the lower states in the valence band are also very much dependent on the direction in the reciprocal space.

The composition of the calculated bands can be understood with the help of the partial and total density of states (DOS) diagrams, which are exhibited in Fig. 3.

The conduction band is about 5 eV wide and consists of two sub-bands. The lower one – from about 4.3 eV to about 5.5 eV – is formed by the Nb 4d states, whereas the upper one from about 6 eV to about 8.5 eV is due to the La and Ba 5d states. A minor contribution from the O 2p states is also evidenced, due to the hybridization effects, preliminarily between the O and Nb ions.

The valence band, which is about 5 eV wide, is composed of the O 2p states, to which the Nb 4d states make a small contribution due to the aforementioned hybridization effect. There are three narrow bands from −15 to −10 eV; which are produced by the 5p states of Ba and La, together with the O 2s states. Finally, the Ba 5s states are peaked at about −26 eV, the Nb 4p states—at about −30 eV, and the Nb 4s states—at about −54 eV.

The optical properties of a solid can be described by its dielectric function $\varepsilon=\mathrm{Re}(\varepsilon)+i\,\mathrm{Im}(\varepsilon)$, with its imaginary part being proportional to the absorption spectrum and its real part determining the value of the refractive index n. Fig. 4, which exhibits the calculated dielectric function for Ba_2LaNbO_6, allows for the estimation of the refractive index $n=\sqrt{\mathrm{Re}(\varepsilon)}_{E=0}=1.7$. A wide band in the calculated imaginary part of dielectric function (from 4 to 11 eV; see Fig. 4) is related to the absorption from the valence to the conduction band, its width is approximately equal to the sum of widths of both bands.

The calculated Mulliken charges [17] for all ions are as follows: Ba +1.06, La +2.79, Nb +1.17, O −1.02. A large difference between the calculated Mulliken charges and formal charges for Nb and O emphasizes the high covalency of the Nb–O bonding. On the contrary, the calculated charge of the La ions is close to their formal charge (+3), which indicates that these ions are connected to the crystal lattice by mostly ionic bonds.

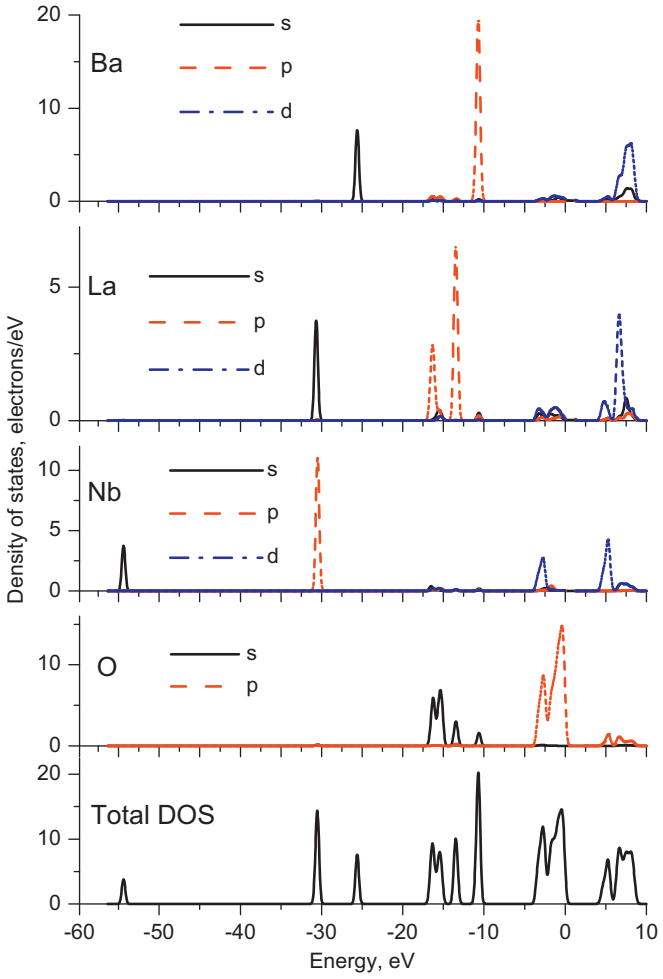

Fig. 3. Partial and total density of states (DOS) for Ba_2LaNbO_6.

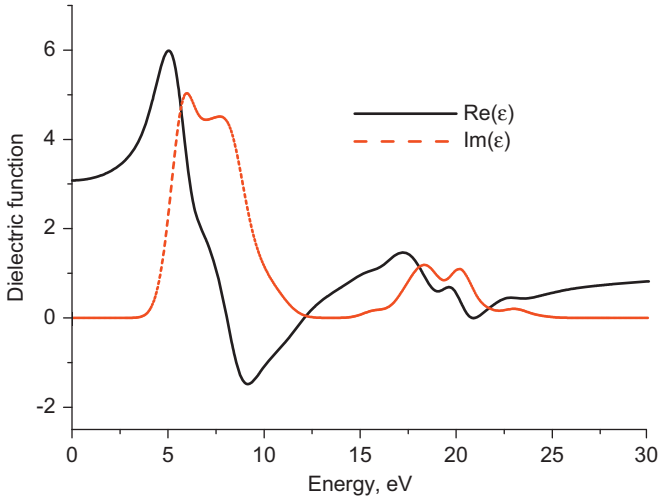

Fig. 4. Calculated real part (solid line) and imaginary part (dashed line) of the dielectric function for pure Ba_2LaNbO_6.

4. Electronic and optical properties of Mn-doped Ba_2LaNbO_6

The calculated band structure of Ba_2LaNbO_6 activated with Mn^{4+} is shown in Fig. 5. To model the Mn^{4+} influence on the electronic properties of the host crystal, we considered the $2 \times 1 \times 1$ supercell with one Nb ion replaced by Mn. Such a cluster would correspond to 25% concentration of doping ions, which

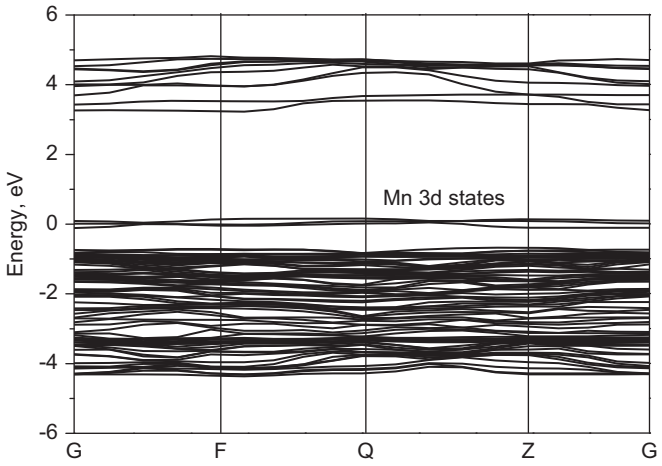

Fig. 5. Calculated band structure of $Ba_2LaNbO_6:Mn^{4+}$.

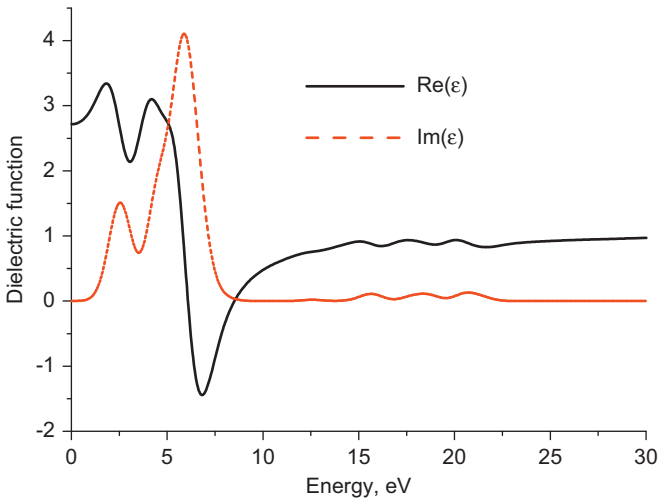

Fig. 6. Calculated real part (solid line) and imaginary part (dashed line) of dielectric function for $Ba_2LaNbO_6:Mn^{4+}$.

considerably exceeds the experimental concentration. However, such a supercell was used due to computational limitations. In addition, the main point of calculating the band structure of the doped crystal was to estimate the position of the lowest manganese 3d states with respect to the band structure of the host material. There is a striking difference between Figs. 2 and 5: the Mn 3d states appear within the host lattice band gap, with the lowest state being about 1.0 eV above the top of the valence band.

A nearly flat profile of the Mn 3d states in the host's band gap suggests a high degree of localization of these states around the Mn ions. The presence of the Mn^{4+} 3d states within the band gap of Ba_2LaNbO_6 manifests itself in the optical properties as well. Fig. 6 shows the calculated dielectric function for the Mn^{4+} activated crystal. Again, there is a considerable difference between Figs. 4 and 6: an absorption peak at about 1–2 eV is due to the Mn states; in the same spectral range there is an anomalous dispersion region (in the real part of the dielectric function).

Since the calculations of the multiplet structure of impurity ion's energy levels are impossible in CASTEP, we have turned to the semi-empirical crystal field theory, to analyze in more details the excitation and luminescence spectra of Mn^{4+}-activated Ba_2LaNbO_6. This is discussed in the next section.

5. Crystal field calculations for Mn^{4+}-activated Ba_2LaNbO_6

The energy levels of impurity ions with an unfilled d-shell (in our case, Mn^{4+} ion with $3d^3$ electron configuration) in a crystal field (CF) of arbitrary symmetry can be represented by the eigenvalues of the following CF Hamiltonian [[18], or any standard book on crystal field theory]:

$$H = \sum_{p=2,4} \sum_{k=-p}^{p} B_p^k O_p^k, \tag{1}$$

where O_p^k are the suitably chosen linear combinations of the irreducible tensor operators acting on the angular parts of the impurity ion's wave functions (exact definition of the operators used in the exchange charge model (ECM) can be found in Ref. [18]), and B_p^k are the crystal field parameters (CFPs), which can be calculated from the crystal structure data and thus, in general, they include all the structural and geometrical information about the host lattice and in particular reflect in a certain sense arrangement of the host lattice ions around the impurity site. The Hamiltonian Eq. (1) is defined in the space spanned by all wave functions of the free ion's LS terms (which arise due to the Coulomb interaction between electrons of an impurity ion). In the ECM, the CFPs are written as a sum of two terms [18]:

$$B_p^k = B_{p,q}^k + B_{p,S}^k, \tag{2}$$

where the first term:

$$B_{p,q}^k = -K_p^k e^2 \langle r^p \rangle \sum_i q_i \frac{V_p^k(\theta_i, \varphi_i)}{R_i^{p+1}}, \tag{3}$$

is the point charge contribution to the CFPs, which arises from the electrostatic interaction between the central ion and the lattice ions enumerated by index i with charges q_i and spherical coordinates, R_i, θ_i, φ_i (with the reference system centered at the impurity ion itself). The averaged values $\langle r^p \rangle$, where r is the radial coordinate of the d electrons of the optical center, can be obtained either from the literature or calculated numerically, using the radial parts of the corresponding ion's wave functions. The values of the numerical factors K_p^k, γ_p (the latter appears in Eq. (4) below), the expressions for the polynomials V_p^k and the definitions of the operators O_p^k can all be found in Ref. [18] and thus are not shown here for the sake of brevity. The second term of Eq. (2) is proportional to the overlap between the wave functions of the central ion and ligands and thus includes all covalent effects. It can be calculated using the following equation:

$$B_{p,S}^k = K_p^k e^2 \frac{2(2p+1)}{5} \sum_i (G_s S(s)_i^2 + G_\sigma S(\sigma)_i{}^2 + \gamma_p G_\pi S(\pi)_i^2) \frac{V_p^k(\theta_i, \varphi_i)}{R_i}, \tag{4}$$

with $S(s)$, $S(\sigma)$, $S(\pi)$ corresponding to the overlap integrals between the d-functions of the central ion and p- and s-functions of the ligands: $S(s) = \langle d0|s0 \rangle$, $S(\sigma) = \langle d0|p0 \rangle$, $S(\pi) = \langle d1|p1 \rangle$. The G_s, G_σ, G_π entries are dimensionless adjustable parameters of the model, whose values are determined from the positions of the first three absorption bands in the experimental spectrum. They can be approximated to a single value, i.e. $G_s = G_\sigma = G_\pi = G$, which then can be estimated from one absorption band only [18].

The main advantages of the ECM are the following: (i) a small number of fitting parameters; (ii) the opportunity to calculate the CFPs and energy levels of the impurity ions in crystals without invoking any assumptions about the impurity center symmetry, but by using only crystal structure data and (iii) the possibility to treat the covalent effects quantitatively (via the calculations of the overlap integrals).

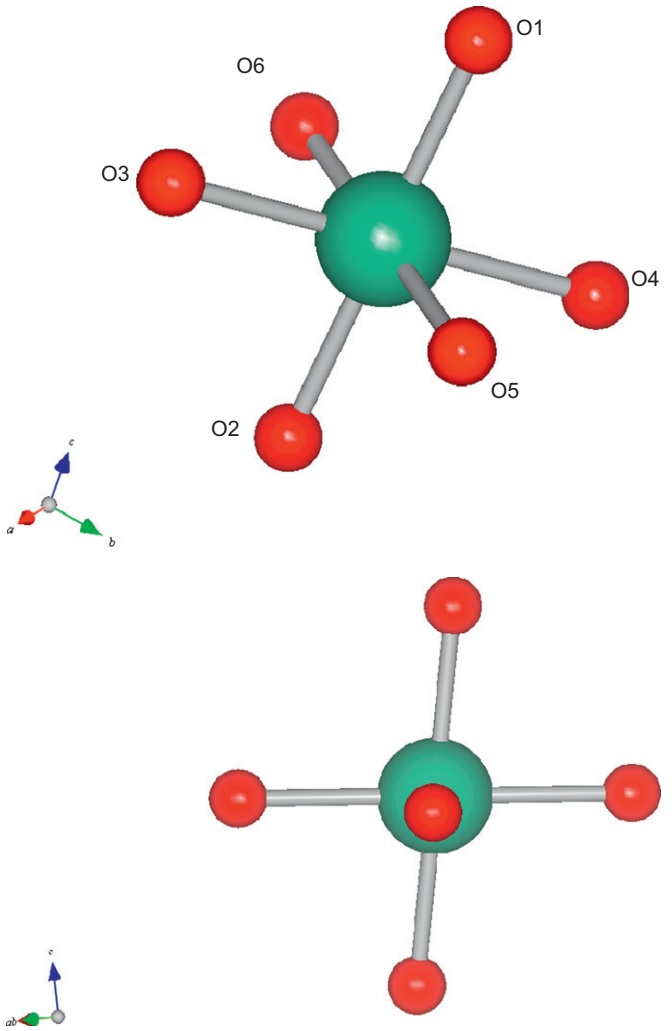

Fig. 7. The view of the NbO_6 complex in Ba_2LaNbO_6 (top) and its side view (bottom) demonstrating non-orthogonality of the equatorial plane of the complex and its z axis.

In the present work the calculations of the crystal field parameters were performed using a large cluster consisting of 36,000 ions, which ensure proper convergence of the crystal lattice sums. The overlap integrals between the Mn^{4+} and O^{2-} ions were calculated using the corresponding wave functions from Refs. [19,20].

Since the Mn^{4+} ion substitute for the Nb^{5+} ion, we now consider in more details the symmetry properties of the NbO_6 complex in Ba_2LaNbO_6 (Fig. 7). Geometrical consideration of the interatomic distances and angles in this complex leads to the following results: the O1–Nb and O2–Nb distances are 1.96 Å, the O3–Nb, O4–Nb, O5–Nb, O6-Nb are all 2.015 Å. The O1–Nb–O3, O1–Nb–O5, O2–Nb–O4, and O2–Nb–O6 angles are 94.8°. The O1–Nb–O4, O1–Nb–O6, O2–Nb–O3, and O2–Nb–O5 angles are 85.2°. Therefore, if the plane containing the O3, O4, O5, O6 oxygen ions (all of which are at the same distance from the central Nb ion) is taken as the equatorial plane and if the O1–Nb–O2 direction is taken as the axial direction of the considered octahedral complex, such a plane and such an axis are not perpendicular to each other (an illustration to this fact is given by a side view of the NbO_6 complex also shown in Fig. 7).

The O3–Nb–O6 and O4–Nb–O5 angles in the chosen equatorial plane are 81.8°, and two remaining angles O4–Nb–O6 and O3–Nb–O5 are 98.2°.

For further consideration of geometrical properties of the Nb site, the Cartesian coordinates of the Ba_2LaNbO_6 crystal lattice were extracted using the VESTA program [21] in the system of reference, whose origin is at the Nb site and the x and y axes coincide with the crystallographic a and b axes, and the z axis is perpendicular to the yx plane (in fact, the z axis practically coincides with the c crystallographic axis, since the angle $\beta=90.348^\circ$ is very close to 90°). The coordinates of the six nearest oxygen ions surrounding the Nb^{5+} ion are given in Table 1. After having extracted the ionic positions, we rotated the system of reference about its y axis to make a new z axis coincide with the O1-Nb–O2 direction (in this new system of reference two oxygen ions with the Nb–O distances of 1.96 Å are at the z axis; the "new" y coordinates are equal to the "old" ones). The "new" coordinates of the nearest oxygen ions surrounding the Nb^{5+} site are given in Table 1 (in the parenthesis).

On the basis of the performed analysis (supported by Fig. 7 and Table 1), we arrive at the conclusion that the local symmetry of the Nb^{5+} site is C_i.

Table 2 summarizes the calculated non-zero CFPs values, which were calculated in the above-described "new" system of reference with taking into account contribution of 36,000 ions for getting proper convergence of the crystal lattice sums. Table 2 summarizes the calculated CFPs values. They were used to diagonalize the crystal field Hamiltonian in the space spanned by the wave functions of all 8 LS terms of the $3d^3$ electron configuration. The calculated energy levels are given in Table 3 (only the lowest energy levels are shown, from the experimentally studied spectral range).

The experimental excitation and emission spectra of Mn^{4+} in Ba_2LaNbO_6 were assigned as follows [9]: the spin-allowed transitions, $^4A_{2g}(^4F)$–$^4T_{2g}(^4F)$ at 507 nm (19,724 cm^{-1}) and $^4A_{2g}(^4F)$–$^4T_{1g}(^4F)$ at 380 nm (26,316 cm^{-1}) in the excitation spectrum and the spin-forbidden transition $^2E_g(^2G)$–$^4A_{2g}(^4F)$ at 658 and 683 nm (15,198 and 14,641 cm^{-1}, respectively). It should be pointed out that the assignment of the 380 nm band in the excitation spectrum exclusively to $^4A_{2g}(^4F)$–$^4T_{1g}(^4F)$ optical transition may not necessarily be correct since the $O^{2-}\rightarrow Mn^{4+}$ charge transfer transition [3] can overlap the $^4A_{2g}(^4F)$–$^4T_{1g}(^4F)$ excitation band in this wavelength region.

Table 1
The coordinates (all in Å) of the six nearest oxygen ion surrounding the Nb^{5+} site in Ba_2LaNbO_6 before and after (in parenthesis) rotation of the system of reference. See text for more details.

	x	y	z
Nb^{5+}	0.0	0.0	0.0
O	0.51534 (0.0)	0.0	−1.8929 (−1.9618)
O	−0.51534 (0.0)	0.0	1.8929 (1.9618)
O	1.3077 (1.3093)	−1.5228	0.1807 (−0.1689)
O	−1.3077 (−1.3093)	−1.5228	−0.1807 (0.1689)
O	−1.3077 (−1.3093)	1.5229	−0.1807 (0.1689)
O	1.3077 (1.3093)	1.5229	0.1807 (−0.1689)

Table 2
The crystal field (in Stevens normalization) and Racah parameters (in cm^{-1}) for Mn^{4+} in Ba_2LaNbO_6. G is the dimensionless ECM parameter.

	$B^k_{p,q}$	$B^k_{p,S}$	B^k_p
B^0_2	1002.2	1425.3	2427.5
B^1_2	−5847.4	−4342.1	−10,189.5
B^2_2	−4056.6	−2962.7	−7019.3
B^0_4	609.1	4717.1	5326.2
B^1_4	562.2	4032.5	4594.7
B^2_4	247.3	1781.4	2028.7
B^3_4	1720.5	12,380.9	14,101.3
B^4_4	−2735.4	−20,731.2	−23,466.6
G (ECM parameter)	8.0		
B	670		
C	3290		

Table 3
Calculated and experimental energy levels (in cm^{-1}) of Mn^{4+} in Ba_2LaNbO_6.

Energy levels (O_h group notation and "parent" LS term)	Calculated	Experiment [9]
$^4A_{2g}(^4F)$	0	
$^2E_g(^2G)$	14,688, 14,706	~14,680
$^2T_{1g}(^2G)$	14,877, 15,694, 15,753	~15,190
$^4T_{2g}(^4F)$	18,499, 20,022, 20,262	~20,000
$^2T_{2g}(^2G)$	21,866, 22,363, 23,915	
$^4T_{1g}(^4F)$	25,337, 26,805, 29,206	~25,000
$^2A_{1g}(^2G)$	32,111	
…	…	…
$^4T_{1g}(^4P)$	40,100, 44,095, 45,424	

A very important characteristic of a particular electron transition is the energy location of the zero phonon line (ZPL). The energy position of the ZPL for the two excitation bands in Fig. 8, is estimated from the following equation [22,23]:

$$I_n^{ex} = I_0^{ex}\exp(-\overline{n})\frac{(\overline{n})^n}{n!}. \quad (5)$$

In this equation I_0^{ex} is the ZPL intensity, $\overline{n}$ is the mean phonon number, and I_n^{ex} is the intensity of the nth vibronic side band. The ZPL positions for the $^4T_{2g}$ and $^4T_{1g}$ excitation bands are 17,700 (with 5 phonons of 466 cm^{-1} [9]) and 22,600 cm^{-1} (with 8 phonons of 466 cm^{-1} [9]), which can be compared with the corresponding values for Mn^{4+} in Na_2SiF_6 19,700 and 23,400 cm^{-1}, respectively [24].

As follows from Fig. 8, the lowest excitation band $^4A_{2g}(^4F)$–$^4T_{2g}(^4F)$ is reproduced practically perfectly. At the same time, the calculated second excitation band appears to be narrower in comparison with the experimental one. This may be explained by the above-mentioned $O^{2-}\rightarrow Mn^{4+}$ charge transfer transitions. On the other hand, the presence of the $^2T_{2g}$ states at about 22,000–23000 cm^{-1} may also contribute to the experimental excitation bands broadening, since the spin-forbidden $^4A_{2g}(^2G)$–$^2T_{2g}(^2G)$ transitions can borrow intensity from the spin-allowed $^4A_{2g}(^4F)$–$^4T_{2g}(^4F)$ transition through the spin–orbit coupling mechanism, thus leading to a considerable widening of the second excitation band in Fig. 8.

6. Conclusions

We have presented in this paper detailed combined analysis of the electronic and optical properties of pure and Mn^{4+} activated Ba_2LaNbO_6, based on the ab initio and semi-empirical methods of calculations. Detailed analysis of the geometrical structure of the NbO_6 complex showed that the local symmetry of the Nb^{5+} site (occupied by the Mn^{4+} ions after doping) is C_i. The calculated energy levels of the six-fold coordinated Mn^{4+} ion in Ba_2LaNbO_6 are in good agreement with the experimental data that has been presented in the literature. The fitting of the excitation bands allows for the estimation of the zero-phonon lines energy and averaged number of phonons involved into the excitation transitions. The so obtained values are consistent with parameters reported for the Mn^{4+} ion in the archival literature. To the best of the authors' knowledge, the present paper represents the first

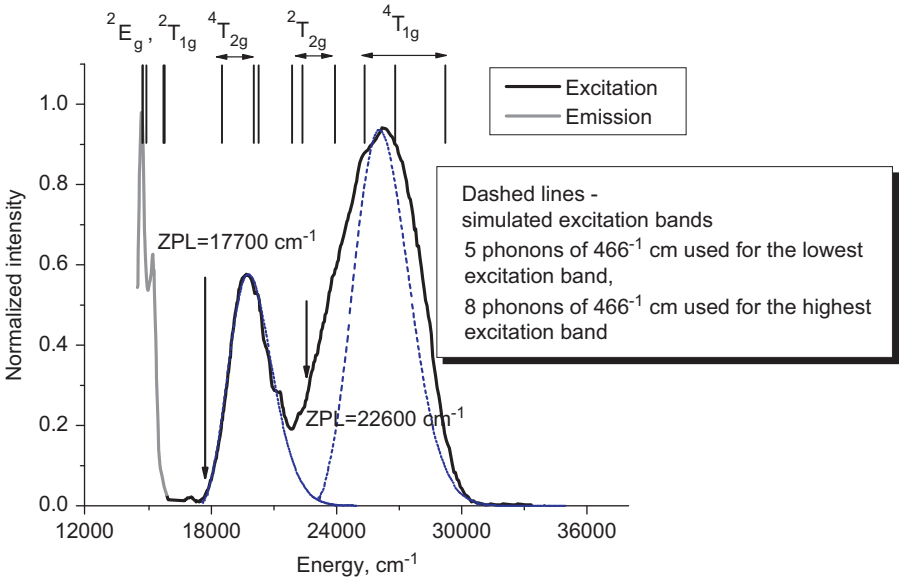

Fig. 8. The emission and excitation spectra (gray and black lines, respectively) of Mn^{4+} activated Ba_2LaNbO_6 (after Ref. [9]) in comparison with the calculated energy levels of Mn^{4+} (vertical lines) and simulated excitation bands (blue dashed lines). Parameters of fits (ZPL energies and effective number of phonons) are shown in the figure. (For interpretation of the references to color in this figure legend, the reader is referred to the web version of this article.)

consistent ab initio and crystal field analysis of optical properties of the $Ba_2LaNbO_6:Mn^{4+}$ system.

Such a combined simultaneous application of the ab initio and semi-empirical models to one host is a powerful tool for getting a complementary and more complete description of the optical and physical properties of the considered system.

Acknowledgment

Prof. Ü. Lille (Tallinn University of Technology) is thanked for allowing to use the Materials Studio package. M.G. Brik's research was supported by European Social Fund's Doctoral Studies and Internationalization Program DoRa.

References

[1] K.H. Butler, Fluorescent Lamp Phosphors, Pennsylvania State University Press, University Park, PA, 1980.
[2] A.M. Srivastava, T.F. Soules, fourth ed.,Luminescent Materials (Phosphors), Kirk-Othmer Encyclopedia of Chemical Technology, vol. 15, John Wiley and Sons, New York, 1995.
[3] A.M. Srivastava, W.W. Beers, J. Electrochem. Soc. 143 (1996) L203.
[4] E.V. Radkov, L.S. Grigorov, A.A. Setlur, A.M. Srivastava, United States Patent Application US2006/0169998 A1, 2006.
[5] M.A. Noginov, G.B. Loutts, J. Opt. Soc. Am. B 16 (1999) 3.
[6] G.B. Loutts, M. Warren, L. Taylor, R.R. Rakhimov, H.R. Ries, G. Miller, M.A. Noginov, M. Curley, N. Noginova, N. Kukhtarev, H.J. Caulfield, P. Venkateswarlu, Phys. Rev. B 57 (1998) 3706.
[7] Ya. Zhydachevskii, D. Galanciak, S. Kobyakov, M. Berkowski, A. Kaminska, A. Suchocki, Ya. Zakharko, A. Durygin, J. Phys.: Condens. Matter 18 (2006) 11385.
[8] Ya. Zhydachevskii, A. Durygin, A. Suchocki, A. Matkovskii, D. Sugak, P. Bilski, S. Warchol, Nucl. Instrum. Methods B 227 (2005) 545.
[9] P.A. Tanner, Z. Pan, Inorg. Chem. 48 (2009) 11142.
[10] L.H. Brixner, J. Inorg. Nucl. Chem. 15 (1960) 352.
[11] W.T. Fu, D.J.W. Ijdo, J. Solid State Chem. 179 (2006) 1022.
[12] M.D. Segall, P.J.D. Lindan, M.J. Probert, C.J. Pickard, P.J. Hasnip, S.J. Clark, M.C. Payne, J. Phys.: Condens. Matter 14 (2002) 2717.
[13] J.P. Perdew, K. Burke, M. Ernzerhof, Phys. Rev. Lett. 77 (1996) 3865.
[14] R.D. Shannon, Acta Crystallogr. A 32 (1976) 751.
[15] Z.H. Levine, D.C. Allane, Phys. Rev. B 43 (1991) 4187.
[16] G. Blasse, A. Bril, Z. Phys. Chem. Neue Folge 57 (1969) 3.
[17] R.S. Mulliken, J. Chem. Phys. 23 (1955) 1833.
[18] B.Z. Malkin, in: A.A. Kaplyanskii, B.M. Macfarlane (Eds.), Spectroscopy of Solids Containing Rare-Earth Ions, North-Holland, Amsterdam, 1987, p. 33.
[19] E. Clementi, C. Roetti, At. Data Nucl. Data Tables 14 (1974) 177.
[20] M.V. Eremin, Spectroscopy of Crystals, Nauka, Leningrad, 1989, pp. 30–44 (in Russian).
[21] K. Momma, F. Izumi, J. Appl. Crystallogr. 41 (2008) 653.
[22] J.J. Hopfield, J. Phys. Chem. Solids 10 (1959) 110.
[23] H. Yamamoto, S. Shionoya, W.M. Yen (Eds.), Phosphor Handbook, CRC, Boca Raton, FL, 1999, p. 35.
[24] Y.K. Xu, S. Adachi, J. Appl. Phys. 105 (2009) 013525.